Eur. Phys. J. D **58**, 311–325 (2010)
DOI: 10.1140/epjd/e2010-00109-5

THE EUROPEAN PHYSICAL JOURNAL D

Regular Article

Band structures of a slowly rotating dipolar Bose-Einstein condensate with a quantized vortex along a one-dimensional optical lattice

H.C. Lee[a] and T.F. Jiang

Institute of Physics, National Chiao Tung University, 30010 Hsinchu, Taiwan

Received 31 August 2009 / Received in final form 22 December 2009
Published online 26 April 2010 –

Abstract. We derive the effective Gross-Pitaevskii equation for a slowly rotating dipolar Bose-Einstein condensate (BEC) with a quantized vortex along a one-dimensional optical lattice and calculate its band structures. The band structure of a slowly rotating BEC in a lattice becomes interesting when dipole-dipole interaction (DDI) is involved. Under rotation, a dipolar rotating term emerges from the DDI potential. The dipolar rotating term makes a BEC with an attractive DDI more stable than one with a repulsive DDI. The dipolar rotating term changes and generalizes the definition for the type of BEC, which cannot be simply determined by an s-wave scattering length or an effective contact interaction term. The dipolar rotating term also makes the band structure fascinating and tunable. A so-called swallowtail band structure, i.e., a multi-valued solution due to nonlinear interaction, can either elongate or shrink as the band index increases, in contrast to a non-rotating dipolar BEC system with a monotonic dependence. With the dipolar rotating term, various band structures as well as an attractive BEC without collapse can be easily achieved. We demonstrate that a rotating dipolar BEC system subject to an optical lattice combines features of a crystal and a superfluid and promises wide applications.

1 Introduction

Rotation of a superfluid, which occurs only in the presence of quantized vortices, is one of the differences between superfluids and classical fluids, in addition to zero viscosity and two-fluid behavior (a mixture of superfluid and normal fluid) [1]. A quantized vortex is a singular point about which the velocity of the fluid is inversely proportional to its distance from the vortex; velocity integration along a contour encircling the vortex is quantized in units of h/m_0, where m_0 is the particle mass of the fluid. The study of quantized vortices is closely connected with the quantum Hall effect [2–5] due to the equivalence of the rotation to an effective magnetic field in a Hamiltonian [6], which relates superfluids to a seemingly very different system: a two-dimensional electron gas in a magnetic field [7]. Furthermore, since turbulence can be regarded as a tangle of vortex lines, understanding vortex dynamics, such as reconnection and decay processes, is helpful for studying the difference between quantum and classical turbulences [8,9]. In particular, it is still unclear whether quantum turbulence obeys the Kolmogorov energy spectrum $E(k_v) \sim k_v^{-5/3}$ as classical turbulence does [10–14], where k_v is the wave number of the velocity field.

A Bose-Einstein condensate (BEC) in optical lattices is a versatile system for exploring the quantum phase transition from superfluid to Mott insulator [15], spin-wave excitation [16], and spinor condensates [17] such as those in the ferromagnetic, polar, and cyclic phases. In optical lattices, a BEC shares many of the properties of electrons in a crystal structure involving Bloch oscillation, Landau-Zener tunneling [18,19], intra (inter) band dynamics, etc. However, a BEC has a unique feature that never occurs in a solid state: while being periodically modulated by a one-dimensional (1D) optical lattice, the BEC density can rotate around a vortex line along the optical lattice, as shown in Figure 1. For comparison, although helium superfluid (He II) can also rotate around a vortex line, the helium density cannot be periodically modulated as that of a BEC in an optical lattice can. Otherwise, a BEC is well described by the mean-field theory, but He II is not, due to the strongly correlated interaction. Thus, its substantial differences from He II make a BEC more significant for exploring the quantum Hall effect in superfluids [2–5] and quantum turbulence [10–14]. Hence, knowledge regarding the band structure of a rotating BEC along an optical lattice is essential; however, current understanding is still limited.

Recently, a new species of dipolar BEC was experimentally realized with ^{52}Cr [20] and attracted considerable interest [21–26]. ^{52}Cr is a spin-3 boson with electronic

[a] e-mail: hclee@mail.nctu.edu.tw

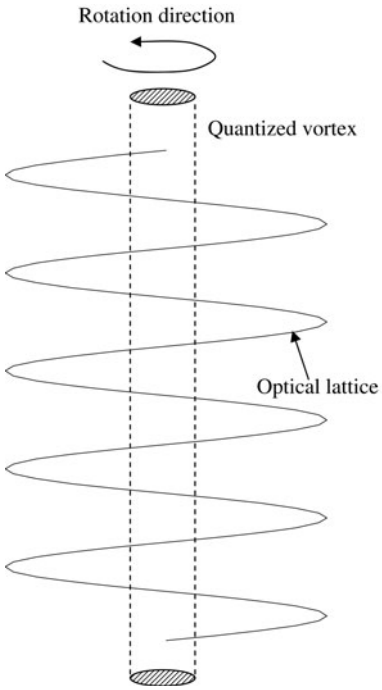

Fig. 1. Schematic diagram for rotating BECs with a vortex line along a 1D optical lattice.

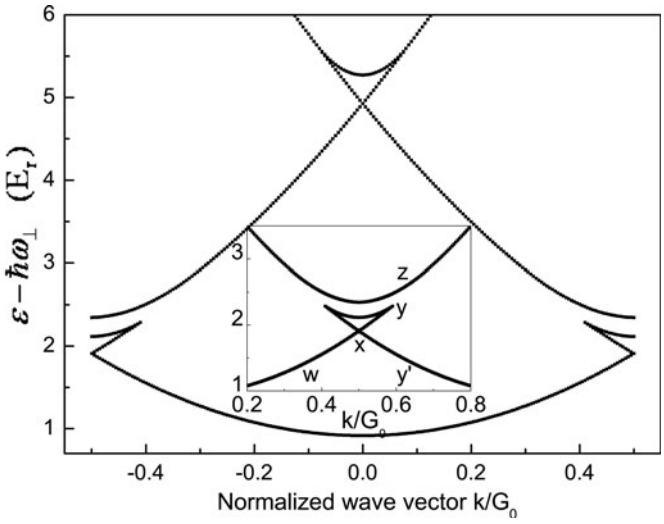

Fig. 2. Band structure demonstrates the swallowtail dependence on the band index for a non-rotating dipolar BEC in a 1D optical lattice. The BEC is repulsive, the DDI is attractive at $\gamma = 0^\circ$, $a_s = 1575a_B$, $a_\perp = 0.523$ μm, $d = 400$ nm, $V_0 = 0.5E_r$, $n = 5.2n_{c,nr}$, and $n_{c,nr} = 1.3 \times 10^7$ m^{-1}.

spin $J = 3$ and nuclear spin $I = 0$, whose dipole-dipole interaction (DDI) is much stronger than that of alkali atoms. In contrast to the contact interaction in a BEC, the DDI is long ranged and anisotropic (partially attractive). The long-ranged behavior probably gives rise to a density wave [21], a supersolid [22] (a mixture of density wave and superfluid), and a series of transitions between vortex lattices of distinct symmetries involving triangular, square, striped and bubble phases as the DDI varies [23]. Meanwhile, the anisotropic behavior offers an opportunity to construct a stable attractive BEC in optical lattices by adjusting the dipolar orientation angle [24], which is helpful for the study of a super Tonks-Girardeau (TG) gas [25], i.e., a strongly correlated state with neither Fermi-Dirac nor Bose-Einstein statistics, in contrast to a TG gas, which consists of a repulsive BEC [27]. Due to these useful phenomena, the band structure of a dipolar BEC is expected to be particularly interesting when the species rotates.

In this paper, we derive the effective Gross-Pitaevskii equation (GPE) for the rotating dipolar BEC system shown in Figure 1 and calculate its band structure. A cigar-shaped trap for the BEC system is considered. Integrating the transverse part of the spatial wave function yields an effective quasi-1D GPE. We found that rotation decreases the contact interaction, and that the DDI potential can be reduced to a dipolar contact term and a dipolar rotating term associated with the second spatial derivative of the BEC density. Interestingly, the dipolar rotating term has an energy dependence opposite to that of the dipolar contact term. The dipolar rotating term is positive for an attractive DDI and negative for a repulsive DDI; i.e., the dipolar rotating term makes a BEC with an attractive DDI more stable than one with a repulsive DDI. Therefore, the rotation can be used to construct an attractive BEC without collapse, in addition to tuning the dipolar orientation angle. The dipolar rotating term also has a special effect on the band structure. A multi-valued solution, also called a loop or a swallowtail structure [28–30], has been identified in a band structure around the zone boundary and zone center as shown in Figure 2 in the past. The width of the swallowtail structure always decreases as the band index increases. Intriguingly, such monotonic dependence does not hold for a rotating dipolar BEC system due to the special property of the dipolar rotating term. By adjusting the type of BEC and DDI (repulsive or attractive), the swallowtail structure can either elongate or shrink as the band index increases. The behavior provides a new degree of freedom to study nonlinear phenomena such as Landau-Zener tunneling [18,19] and gap solitons [31,32], as well as intra (inter) subband dynamics and optical applications in the band structure of a BEC.

The rest of this paper is organized as follows: in Section 2, the formulation of a rotating dipolar BEC in optical lattices is derived from a three-dimensional (3D) time-independent GPE with a cigar-shaped trap. In Section 3, a solution method based on the central equation with many-mode expansion is described. In Section 4, the results and interesting Bloch functions are presented, and several applications of swallowtail band structures are discussed. Finally, conclusions are drawn in Section 5.

2 Formulation

In a frame rotating with angular frequency Ω around the z-axis, the time-independent GPE for a system of $N_{\rm atom}$ aligned dipolar atoms in a cigar-shaped trap potential and

in a 1D lattice along the rotating axis, as shown in Figure 1, is given by [33,34]

$$\mu\Psi(\mathbf{r}) = \left[-\frac{\hbar^2}{2m}\nabla^2 + V_{trap}(\mathbf{r}) - \Omega L_z + g_s|\Psi(\mathbf{r})|^2 + g_d\int d\mathbf{r}' V_d(\mathbf{r},\mathbf{r}')|\Psi(\mathbf{r}')|^2\right]\Psi(\mathbf{r}), \quad (1)$$

where $V_{trap}(\mathbf{r}) = m\omega_\perp^2\rho^2/2 + V_0\sin^2(\pi z/d)$, $g_s = 4\pi\hbar^2 a_s/m$, $g_d = \mu_0\mu_m^2/4\pi$, $L_z = -i\hbar\partial_\phi$, m is the atomic mass, $\omega_\perp$ is the transverse trap frequency, ρ is the radius in cylindrical coordinates, d is the optical lattice constant, a_s is the s-wave scattering length, and μ_m is the atomic magnetic dipole moment. Note that in a cigar-shaped trap, the trap frequency for the axial direction is much smaller than the transverse frequency and thus is neglected. The DDI potential can be written as

$$V_d(\mathbf{r},\mathbf{r}') = \frac{1}{|\mathbf{r}-\mathbf{r}'|^3} - 3\frac{[\hat{\mathbf{p}}\cdot(\mathbf{r}-\mathbf{r}')]^2}{|\mathbf{r}-\mathbf{r}'|^5}, \quad (2)$$

where $\hat{\mathbf{p}}$ denotes the unit vector of the dipolar alignment.

The wave function $\Psi(\mathbf{r})$ in a cigar-shaped trap can be written as $\psi_\perp(\rho,\phi)\varphi(z)$. With a single quantized vortex, the transverse part of the wave function is given by [35]

$$\psi_\perp(\rho,\phi) = \frac{1}{\sqrt{\pi}a_\perp^2}\rho\, e^{i\phi}e^{-\frac{\rho^2}{2a_\perp^2}}, \quad (3)$$

where $a_\perp = \sqrt{\frac{\hbar}{m\omega_\perp}}$. The wave function vanishes at the vortex line and reaches a maximum value at $\rho = a_\perp$. The local flow velocity $\mathbf{v}$ equals $\frac{\hbar}{m\rho}\hat{\phi}$, which satisfies

$$\oint \mathbf{v}\cdot d\mathbf{l} = \int \nabla\times\mathbf{v}\cdot d\mathbf{S} = \frac{h}{m}, \quad (4)$$

where $\nabla\times\mathbf{v} = \frac{h}{m}\delta(\boldsymbol{\rho})\hat{z}$. Thus, quantized circulation is shown, and the irrotational velocity around the vortex except for a singularity at the origin is demonstrated.

The axial part of the wave function satisfies the Bloch theorem

$$\varphi(z) = e^{ikz}\varphi_B(z), \quad (5)$$

where k is the crystal momentum within the first Brillouin zone $[-\frac{\pi}{d},\frac{\pi}{d}]$. $\varphi_B(z)$ is the Bloch function that satisfies the periodic condition $\varphi_B(z+d) = \varphi_B(z)$.

Multiplying equation (1) by the transverse part of the wave function $\psi_\perp(\rho,\phi)$ and then integrating it over the transverse cross section spanned by the area $\rho\,d\rho\,d\phi$ yields

$$(\mu - 2\hbar\omega_\perp + \hbar\Omega)\varphi(z) = \left[-\frac{\hbar^2}{2m}\frac{d^2}{dz^2} + V_0\sin^2\left(\frac{\pi z}{d}\right) + \frac{g_s}{4\pi a_\perp^2}|\varphi(z)|^2 + g_d\int\rho d\rho d\phi|\psi_\perp(\rho,\phi)|^2\int d\mathbf{r}' V_d(\mathbf{r},\mathbf{r}')|\Psi(\mathbf{r}')|^2\right]. \quad (6)$$

We can see that the transverse part of the wave function modifies the coupling constant of the contact interaction, which is half that a non-rotating BEC [24]. Thus, rotation lowers the contact interaction term. We now treat the nonlocal dipolar potential. First, we define it as

$$V_{\text{nonlocal}}(\mathbf{r}) = \int d\mathbf{r}' V_d(\mathbf{r},\mathbf{r}')|\Psi(\mathbf{r}')|^2. \quad (7)$$

Here the DDI potential $V_d(\mathbf{r},\mathbf{r}')$ depends on the relative position $\mathbf{r}-\mathbf{r}'$. Thus, equation (7) is in the convolved form and can be treated using the convolution theorem

$$V_{\text{nonlocal}}(\mathbf{r}) = \frac{1}{8\pi^3}\int d\mathbf{q}U_d(\mathbf{q})n(\mathbf{q})e^{-i\mathbf{q}\cdot\mathbf{r}}, \quad (8)$$

where we have

$$U_d(\mathbf{q}) = \int d\mathbf{r}V_d(\mathbf{r})e^{i\mathbf{q}\cdot\mathbf{r}} \approx -\frac{4\pi}{3}(1-3\cos^2\alpha), \quad (9)$$

where α is the angle between the vector $\mathbf{q}$ and the aligned dipole [36].

The density function in momentum space can be expressed as

$$\begin{aligned} n(\mathbf{q}) &= \int d\mathbf{r}|\Psi(\mathbf{r})|^2 e^{i\mathbf{q}\cdot\mathbf{r}} \\ &= \int\rho\,d\rho\,d\phi|\psi_\perp^2(\rho,\phi)|^2 e^{iq_\rho\rho\cos(\theta-\phi)}\int dz|\varphi(z)|^2 e^{iq_z z} \\ &\equiv n_\perp(q_\rho,\theta)n_\parallel(q_z), \end{aligned} \quad (10)$$

where the transverse part of the density function in momentum space is given by

$$n_\perp(q_\rho,\theta) = \left(1-\frac{a_\perp^2}{4}q_\rho^2\right)e^{-\frac{a_\perp^2}{4}q_\rho^2}. \quad (11)$$

The axial part of the density function in momentum space $n_\parallel(q_z)$ can be derived using the periodic property; its expression is given in reference [24]. A useful point is that $n_\parallel(q_z)$ is localized at small momentum with $\sim\sin(q_z d)/(q_z d)$ dependence.

With the nonlocal dipolar potential $V_{\text{nonlocal}}(\mathbf{r})$, we can define the effective dipolar potential for the last term on the right-hand side of equation (6)

$$V_{eff}(z) = \int\rho\,d\rho\,d\phi|\psi_\perp(\rho,\phi)|^2\,V_{\text{nonlocal}}(\mathbf{r}). \quad (12)$$

Substituting the nonlocal dipolar potential shown in equation (8) into equation (12) yields

$$\begin{aligned} V_{eff}(z) &= \frac{1}{6\pi^2}\int d^3\mathbf{q}(-1+3\cos^2\alpha)n_\perp^2(q_\rho,\theta)n_\parallel(q_z)e^{-iq_z z} \\ &\equiv V_1(z) + V_2(z), \end{aligned} \quad (13)$$

where we define

$$V_1(z) \equiv \frac{-1}{6\pi^2}\int d^3\mathbf{q}n_\perp^2(q_\rho,\theta)n_\parallel(q_z)e^{-iq_z z}, \quad (14a)$$

$$V_2(z) \equiv \frac{1}{2\pi^2}\int d^3\mathbf{q}\cos^2\alpha n_\perp^2(q_\rho,\theta)n_\parallel(q_z)e^{-iq_z z}. \quad (14b)$$

Equation (14a) can be easily worked out as

$$V_1(z) = \frac{-1}{3a_\perp^2}|\varphi(z)|^2. \tag{15}$$

For $V_2(z)$, further manipulation is needed. Without loss of generality, we choose $\hat{\mathbf{p}}$ in the x-z plane and set $\hat{\mathbf{p}}$ as $(\sin\gamma,\ 0,\ \cos\gamma)$, where γ is the angle between $\hat{\mathbf{p}}$ and the z-axis, i.e., $\cos^2\alpha = (q_\rho\cos\theta\sin\gamma + q_z\cos\gamma)^2/(q_\rho^2+q_z^2)$. Putting $\cos^2\alpha$ into equation (14b) then yields

$$\begin{aligned} V_2(z) &= -\frac{P_2(\cos\gamma)}{2\pi}\int dq_z\left[\frac{3}{4}q_z^2 + \frac{a_\perp^2}{8}q_z^4 + f(q_z)\right] \\ &\quad\times n_\parallel(q_z)e^{-iq_z z} \\ &\equiv V_2'(z) + V_2''(z), \end{aligned} \tag{16}$$

where $P_2(\cos\gamma)$ is the second-order Legendre polynomial,

$$f(q_z) = \left(q_z^2 + \frac{a_\perp^2}{2}q_z^4 + \frac{a_\perp^4}{16}q_z^6\right)e^{\frac{a_\perp^2}{2}q_z^2}Ei\left(-\frac{a_\perp^2}{2}q_z^2\right), \tag{17}$$

where the exponential integral $Ei(-x)$ is defined as $-\int_x^\infty \exp(-t)/t dt$ for $x>0$,

$$V_2'(z) \equiv -\frac{P_2(\cos\gamma)}{2\pi}\int dq_z\left(\frac{3}{4}q_z^2 + \frac{a_\perp^2}{8}q_z^4\right)n_\parallel(q_z)e^{-iq_z z}, \tag{18a}$$

$$V_2''(z) \equiv -\frac{P_2(\cos\gamma)}{2\pi}\int dq_z f(q_z)n_\parallel(q_z)e^{-iq_z z}. \tag{18b}$$

Equation (18a) can be easily worked out as

$$V_2'(z) = P_2(\cos\gamma)\left(\frac{3}{4}\frac{d^2}{dz^2}|\varphi(z)|^2 - \frac{a_\perp^2}{8}\frac{d^4}{dz^4}|\varphi(z)|^2\right). \tag{19}$$

For $V_2''(z)$, we need an approximation. At a small value of q_z, $f(q_z)\sim 0$, whereas at a large value of q_z, $f(q_z)\sim -2a_\perp^{-2} - q_z^2 - a_\perp^2 q_z^4/8$. Since $n_\parallel(q_z)$ localizes at small momentum with $\sim\sin(q_z d)/(q_z d)$ dependence, the integral of equation (18b) involving the q_z^2 term in $f(q_z)$ shows the dominant value at a small value of q_z, whereas the integral of equation (18b) involving the q_z^4 and q_z^6 terms in $f(q_z)$ shows the dominant value at a large value of q_z. As a result, equation (18b) can be worked out as

$$V_2''(z) = P_2(\cos\gamma)\left(-\frac{d^2}{dz^2}|\varphi(z)|^2 + \frac{a_\perp^2}{8}\frac{d^4}{dz^4}|\varphi(z)|\right). \tag{20}$$

Finally, the effective quasi-1D GPE for a slowly rotating dipolar BEC with a quantized vortex along the 1D optical lattice, as shown in Figure 1, can be written as

$$\begin{aligned} (\mu - 2\hbar\omega_\perp + \hbar\Omega)\varphi(z) = \Bigg\{&\frac{-\hbar^2}{2m}\frac{d^2}{dz^2} + V_0\sin^2\left(\frac{\pi z}{d}\right) \\ &+\frac{1}{a_\perp^2}\left[\frac{g_s}{4\pi} - \frac{g_d}{3}P_2(\cos\gamma)\right]|\varphi(z)|^2 \\ &-\frac{g_d}{4}P_2(\cos\gamma)\frac{d^2}{dz^2}|\varphi(z)|^2\Bigg\}\varphi(z). \end{aligned} \tag{21}$$

The effective GPE has several important characteristics. First, by integrating out the transverse part of the wave function, the DDI potential can be reduced to the dipolar contact term $[-g_d P_2(\cos\gamma)/(3a_\perp^2)]$ and the dipolar rotating term $[-g_d P_2(\cos\gamma)/4]$. The dipolar contact term is half that of a non-rotating dipolar BEC system [24], which is the same as the reduction in the contact term $[g_s/(4\pi a_\perp^2)]$ due to the rotation. The sum of the contact term and the dipolar contact term is called the effective contact term. A repulsive DDI, where the dipolar angle γ satisfies $P_2(\cos\gamma)<0$, strengthens the effective contact term, and an attractive DDI, where the dipolar angle γ satisfies $P_2(\cos\gamma)>0$, weakens the effective contact term. Second, due to the second spatial derivative of the density, the dipolar rotating term is positive for an attractive DDI and negative for a repulsive DDI, i.e., the dipolar rotating term makes BEC with an attractive DDI more stable than one with a repulsive DDI, which is contrary to the effective contact term. Third, since the dipolar rotating term conflicts with the effective contact term, the type of BEC depends on both the effective contact term and the dipolar rotating term. If the energy summed over the effective contact term and the dipolar rotating term over all space is positive, the BEC is repulsive; if the energy summed over the two terms for all space is negative, the BEC is attractive.

3 Solution method

In this section, after deriving the effective GPE for a dipolar BEC rotating slowly around a quantized vortex along a 1D lattice, we describe a method for calculating the corresponding energy band structures. A standard central-equation method [37] taken from solid-state physics is employed with a many-mode expansion for the Bloch function. The central-equation method will be shown to have a better convergence for solutions than the conventional variational method. Meanwhile, the variational method will be used to derive the density criterion for the so-called swallowtail solutions in a band structure because it has an analytic expression.

First, we need to derive the central equation from equation (21). As mentioned above, the axial wave function $\varphi(z)$ can be written in the Bloch form as $e^{ikz}\varphi_B(z)$. The Bloch function $\varphi_B(z)$ can be expanded as a Fourier series due to the periodic property

$$\varphi_B(z) = \sqrt{n}\sum_{\nu=-M}^{M} c_\nu \exp(i\nu G_0 z), \tag{22}$$

where G_0 is the reciprocal lattice vector and equal to $2\pi/d$. n is the atom density, defined as $d^{-1}\int_{-d/2}^{d/2}|\varphi(z)|^2 dz$. $M=1,\ 2,\ 3,\ldots$ represents 3-mode, 5-mode, 7-mode,... expansions, respectively. In general, only a few modes in the expansion are enough to give convergent results.

c_ν satisfies the normalization condition as $\sum_\nu |c_\nu|^2 = 1$

$$\int_{\text{all sites}} |\varphi(z)|^2 dz = N_{\text{site}} \int_{\text{one site}} |\varphi_B(z)|^2 dz = N_{\text{site}}\, dn \sum_\nu |c_\nu|^2 = N_{\text{atom}}, \quad (23)$$

where N_{site} is the number of lattice sites. N_{atom} is the atom number over the lattice.

Substituting the axial wave function $\varphi(z)$ into equation (21) and comparing both sides of equation (21) for each Fourier component yields the required central equation

$$\left[\mu - 2\hbar\omega_\perp + \hbar\Omega - \frac{\hbar^2}{2m}(k+\nu G_0)^2 - \frac{V_0}{2}\right] c_\nu + \frac{V_0}{4}(c_{\nu-1} + c_{\nu+1}) - n\sum_{\nu',\xi}\left[g_{eff}(\gamma) + (\nu-\xi)^2 g_{rot}(\gamma)\right] c_{\nu'} c_\xi c_{\nu+\nu'-\xi} = 0, \quad (24)$$

where $g_{eff}(\gamma) = \frac{1}{a_\perp^2}[\frac{g_s}{4\pi} - \frac{g_d}{3}P_2(\cos\gamma)]$ and $g_{rot}(\gamma) = -\frac{g_d}{4}P_2(\cos\gamma)$.

For a $2M+1$ mode expansion, equation (24) generates the $2M+1$ coupled equations, which are fourth-order nonlinear algebraic equations. These equations can be solved for the $2M$ independent c_ν's and the chemical potential. Given a wave vector k within the first Brillouin zone, solutions with $2M+1$ bands can be obtained. As the chemical-potential band structure is obtained, the energy band structure of the rotating dipolar BEC system can be calculated via the energy functional per atom

$$\varepsilon[\varphi] = (2\hbar\omega_\perp - \hbar\Omega) + \frac{1}{nd}\int_{-d/2}^{d/2} dz \left\{ \frac{\hbar^2}{2m}\left|\frac{d\varphi}{dz}\right|^2 + V_0 \sin^2\left(\frac{\pi z}{d}\right)|\varphi|^2 + \frac{1}{2}g_{eff}(\gamma)|\varphi|^4 + \frac{1}{2}g_{rot}(\gamma)\left[|\varphi|^2\frac{d^2|\varphi|^2}{dz^2} + \frac{1}{2}\varphi^2\frac{d^2\varphi^{*2}}{dz^2} + \varphi\frac{d\varphi}{dz}\frac{d\varphi^{*2}}{dz}\right]\right\}, \quad (25)$$

whose expression in Bloch form with many-mode expansion is given by

$$\varepsilon[\varphi] = 2\hbar\omega_\perp - \hbar\Omega + \frac{\hbar^2}{2m}\sum_\nu c_\nu^2 (k+\nu G_0)^2 + \frac{V_0}{2} - \frac{V_0}{4}\sum_\nu [c_\nu(c_{\nu+1} + c_{\nu-1})] + \frac{n}{2}\sum_{\nu,\nu',\xi} c_\nu c_{\nu'} c_\xi c_{\nu-\nu'+\xi}\Big\{ g_{eff} + g_{rot}G_0^2\big[(\nu-\nu'+\xi)(\nu-\xi) + (\nu-\nu')(\nu-\nu'+2k/G_0)\big]\Big\}. \quad (26)$$

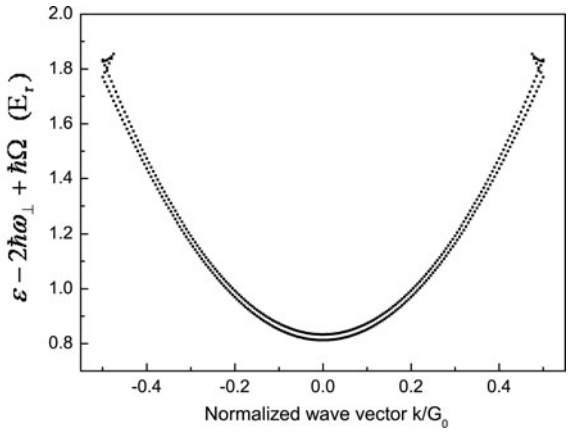

(a)

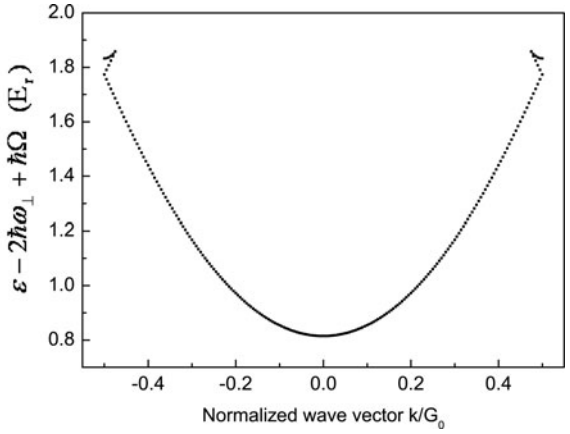

(b)

Fig. 3. Ground band structures from 3-mode expansion for the rotating dipolar BEC by using (a) the variational method and (b) the central-equation method. The BEC is repulsive, the DDI is attractive at $\gamma = 0^\circ$, $a_s = 1575a_B$, $a_\perp = 0.523$ μm, $d = 400$ nm, $V_0 = 1E_r$, $n = 2n_{c,r}$, and $n_{c,r} = 1.7 \times 10^7$ m^{-1}.

Regarding the variational method, the $2M$ independent c_ν's of a $2M+1$ mode expansion are not solved by the central equation in equation (24), but are directly determined by requiring equation (26) to be stationary with respect to the $2M$ independent c_ν's variables.

4 Results and discussions

In practical terms, ^{52}Cr has an atomic magnetic dipole moment of 6 Bohr magnetons. From experimental parameters [38], a transverse trap frequency $\omega_\perp$ of $2\pi \times 712.5$ Hz is used in our numerical calculations. Thus, the transverse trap length is 0.523 μm. Unless otherwise specified, the lattice constant is 400 nm, and the lattice is constructed of lasers with a wavelength of 800 nm. The energy of band structures and the potential height of optical lattices are in units of recoiled energy E_r, defined as $\pi^2\hbar^2/(2md^2)$.

Figures 3a and 3b show the ground band structures from the 3-mode expansion of the rotating dipolar BEC

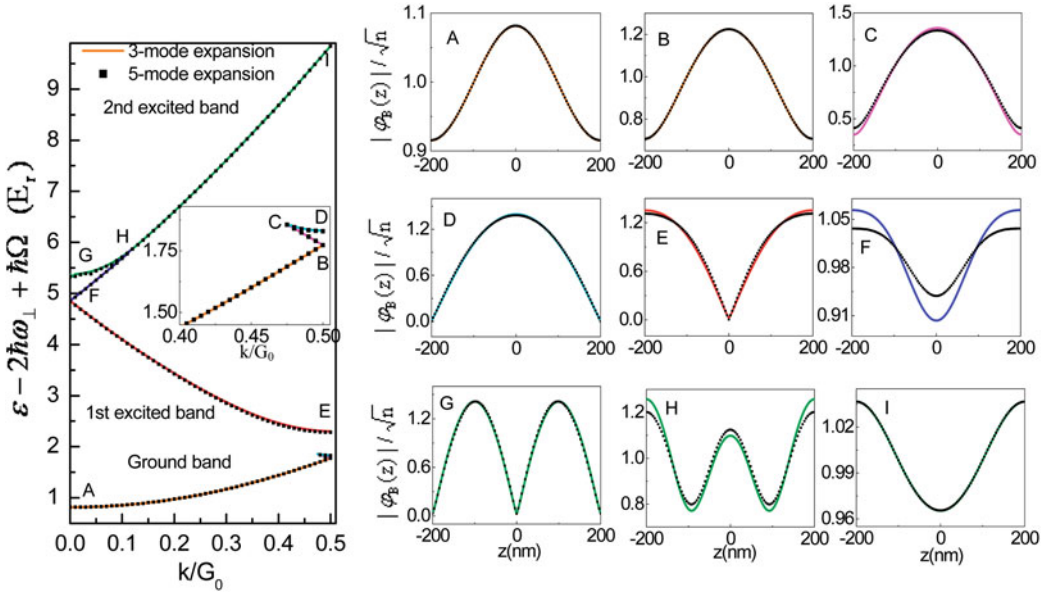

Fig. 4. (Color online) The 3-mode (line) and 5-mode (scatter) band structures for the rotating dipolar BEC. The BEC is repulsive, the DDI is attractive at $\gamma = 0°$, $a_s = 1575a_B$, $a_\perp = 0.523$ μm, $d = 400$ nm, $V_0 = 1E_r$, $n = 2n_{c,r}$, and $n_{c,r} = 1.7 \times 10^7$ m^{-1}. The absolute value of the 3-mode (solid) and 5-mode (dash) Bloch functions at designated points is also shown.

system using the variational method and the central equation, respectively. We use $a_s = 1575a_B$, where a_B is the Bohr radius, $n = 3.4 \times 10^7$ m^{-1} ($= 2n_{c,r}$, defined later), $V_0 = 1E_r$, and the DDI is attractive at $\gamma = 0°$. Two close-lying parabolic bands separated by about 20 meV are shown in Figure 3a. The two separated bands are not correct solutions, but appear due to an insufficient number of modes in the expansion. With more than the 3-mode expansion in the variational method, the two separated bands merge into one. On the other hand, in the same 3-mode expansion, the central equation shows a convergent one-band result, as depicted in Figure 3b, and thus is a better numerical scheme than the variational method. Therefore, in this paper, we use the central equation to calculate band structures. However, the variational method is useful for deriving the density criterion for swallowtail structures around the zone boundary due to its analytic expression. With the 2-mode expansion,

$$\varphi(z) = \sqrt{n}\{\cos\alpha \exp(ikz) + \sin\alpha \exp[i(k - G_0)z]\}, \quad (27)$$

where α is the variational parameter. Using 2-mode expansion in equation (26) and taking variation at the zone boundary yields two solutions: $\cos 2\alpha = 0$ and $\sin 2\alpha = \frac{V_0}{2n(g_{eff} - g_{rot}G_0^2)}$. The latter is related to the swallowtail structure and appears when the atom density exceeds a critical value $n_{c,r} \equiv \frac{V_0}{|2(g_{eff} - g_{rot}G_0^2)|}$. For comparison, the density criterion for a non-rotating dipolar BEC system is given by $n_{c,nr} \equiv \frac{V_0}{|2g_{eff}^{(nr)}|}$, where $g_{eff}^{(nr)}(\gamma) \equiv \frac{1}{a_\perp^2}[\frac{g_s}{2\pi} - \frac{2g_d}{3}P_2(\cos\gamma)]$ is twice as large as $g_{eff}(\gamma)$.

The so-called swallowtail structure or loop structure is a multi-valued function. A certain wave vector around the zone boundary or zone center can map to several states with different energies. At first glance, the multi-valued function may appear inappropriate or unphysical because it is not a one-to-one mapping system. However, in fact, more than a few physical systems show multi-valued behavior. A typical example is band structure, which includes all band information within a Brillouin zone and therefore is multi-valued. Band structure is often viewed as just a convenient presentation for visualization, but the wave vector k actually has a translation symmetry with the reciprocal lattice vector (see Appendix A). Due to this translation symmetry, a semiconductor in which the conduction band minimum and the valence maximum lie at the same wave vector is called a direct band gap; this is an extremely important principle for the physics of optoelectronic devices. Another example is the well-known magnetic hysteretic phenomenon, in which a single magnetic field can map to several magnetic flux densities due to memory effects [39–41]. In the past, the swallowtail structure of a BEC has been considered a generic sign of superfluid hysteresis [42]. Other examples of multi-valued properties exist, such as the transport property in an electronic device called a semiconductor controlled rectifier [43].

Figure 4 shows the band structures of the 3-mode (line) and 5-mode (scatter) expansion of the rotating dipolar Bose system, where the parameters are the same as that in Figure 3b with the condition that the critical density $n_{c,r}$ is 1.7×10^7 m^{-1}. Some interesting Bloch functions are also plotted. The difference between the energies of the 3-mode and 5-mode expansions for the ground band is less than 0.15%, whereas the difference between the two modes for the first excited and the second excited bands is less than 1.05%. Thus, the accuracy of the 3-mode and 5-mode expansions for band structures in our calculation is acceptable. However, the difference in Bloch functions

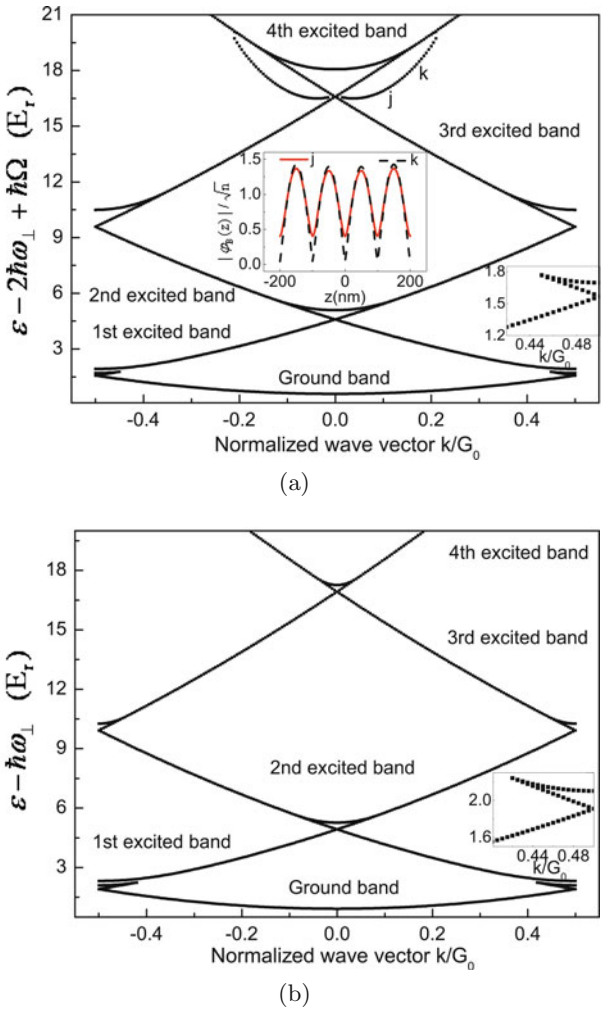

Fig. 5. (Color online) The 5-mode band structures for (a) the rotating and (b) non-rotating dipolar BEC. The BEC is repulsive, the DDI is attractive at $\gamma = 0°$, $a_s = 1575a_B$, $a_\perp = 0.523$ μm, $d = 400$ nm, $V_0 = 0.5E_r$, $n = 4n_{c,r}$, $n_{c,r} = 1.7 \times 10^7$ m^{-1}, and $n_{c,nr} = 1.3 \times 10^7$ m^{-1}. Inset plots show Bloch functions of new solutions at the 4th excited band and enlarged swallowtail around the zone boundary.

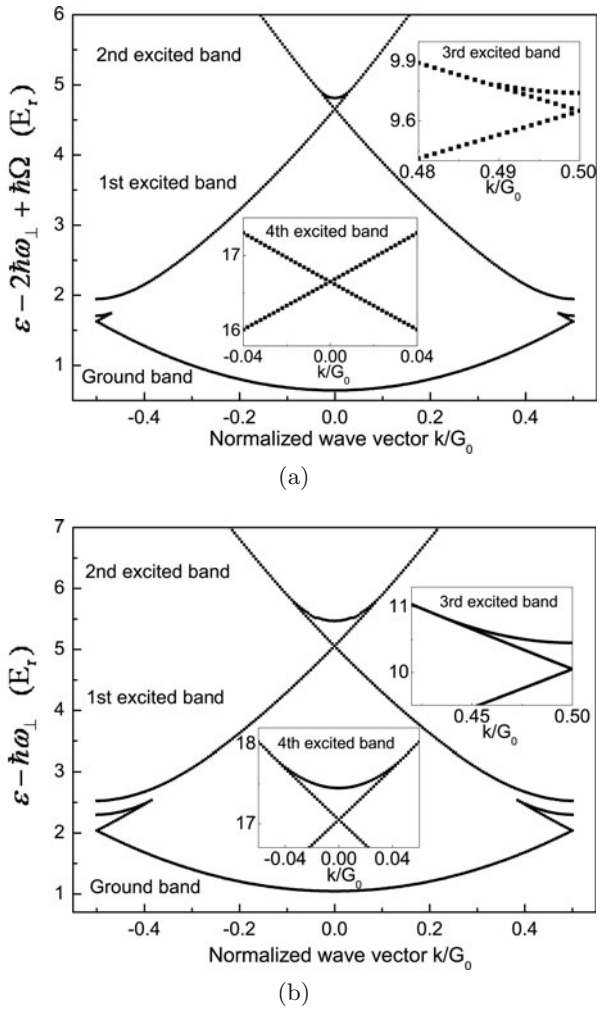

Fig. 6. The 3-mode band structures for (a) the rotating and (b) non-rotating dipolar BEC. The BEC is repulsive, the DDI is repulsive at $\gamma = 60°$, $a_s = 1575a_B$, $a_\perp = 0.523$ μm, $d = 400$ nm, $V_0 = 0.5E_r$, $n = 3n_{c,r}$, $n_{c,r} = 2.7 \times 10^7$ m^{-1}, and $n_{c,nr} = 1.3 \times 10^7$ m^{-1}. Inset plots show swallowtail structures around the boundary of the 3rd excited bands and around the center of the 4th excited bands from the solutions of the 5-mode expansion.

between the two expansions is greater than the energy difference; in particular, the average differences of points C, F and H over the unit lattice are 3.78%, 2.03% and 2.7%, respectively. Thus, for calculations involving Bloch functions, higher-order mode expansion is probably necessary.

Figure 5a shows the 5-mode-expansion band structure of a rotating dipolar BEC system, where the BEC is repulsive, $a_s = 1575a_B$, $n = 4n_{c,r}$, $V_0 = 0.5E_r$, and the DDI is attractive at $\gamma = 0°$. The critical density for the rotating system $n_{c,r}$ is 1.7×10^7 m^{-1}. We choose a slightly low height for the optical lattices to keep the critical density dilute. If V_0 is set to $1E_r$, the critical density becomes 3.4×10^7 m^{-1}, and the atom density increases to 1.36×10^8 m^{-1}, which is relatively high for a BEC. Swallowtail structures appear at the zone boundary and the zone center. Interestingly, the swallowtail structure lengthens with increasing band index. A longer swallowtail appears at the third excited band than at the ground band, while the swallowtail at the fourth excited band is longer than that at the second. Incidentally, a new type of solution at the fourth excited band appears in addition to the swallowtail structure; two samples of the corresponding Bloch function are shown in the inset. For comparison, with all the same conditions, the swallowtail of the non-rotating dipolar BEC system shown in Figure 5b shrinks with increasing band index, where the critical density for the non-rotating dipolar BEC system $n_{c,nr}$ is 1.3×10^7 m^{-1}.

For a rotating system, if the attractive DDI is replaced with a repulsive DDI in a repulsive BEC, the swallowtail shrinks with increasing band index. Figure 6a shows the band structure of a rotating BEC system with a repulsive DDI at $\gamma = 60°$, where $a_s = 1575a_B$, $n = 3n_{c,r}$

and $V_0 = 0.5E_r$. The critical density for the rotating system $n_{c,r}$ is 2.7×10^7 m^{-1}. For comparison, the band structure of a non-rotating dipolar BEC system is shown in Figure 6b with all the same parameters as in Figure 6a. The critical density for the non-rotating system is $n_{c,nr} = 1.3 \times 10^7$ m^{-1}. The swallowtails in both Figures 6a and 6b shrink as the band index increases. Inset plots show swallowtails at the boundary of the third excited bands and at the center of the fourth excited bands. A shorter swallowtail appears at the third excited (fourth excited) band than that at the ground (second excited) band, where the swallowtail at the 4th excited band of the rotating system vanishes. Due to the two-times-lower critical density, the swallowtail of the non-rotating system is longer than that of the rotating system.

Figure 7a shows the 5-mode-expansion band structure of a rotating dipolar BEC system, where the BEC becomes attractive, $a_s = 15a_B$, $n = 3n_{c,r}$, $V_0 = 0.2E_r$, $d = 250$ nm, and the DDI is repulsive at $\gamma = 90°$. Although the scattering length a_s is positive, the BEC is still attractive because the negative dipolar rotating term is much larger than the positive effective contact term. The critical density for the rotating system $n_{c,r}$ is 4.3×10^7 m^{-1}. At atom densities higher than $2n_{c,r}$, the BEC begins to collapse. The band structures of attractive and repulsive BECs are quite different. First, the ground band of an attractive BEC resembles the solution of tight-binding model, where the band curvature (effective mass) is positive around the zone center and negative around the zone boundary. Second, the swallowtail structure of an attractive BEC appears at the boundary of the first excited band and the direction of its swallowtail structure is opposite to that of a repulsive BEC. The above two characteristics are essentially the same as those of the non-rotating attractive BEC system shown in Figure 7b, where $a_s = -1575a_B$, $n = 2n_{c,nr}$, $V_0 = 0.5E_r$, and the DDI is repulsive at $\gamma = 90°$. The critical density for the non-rotating dipolar BEC system $n_{c,nr}$ is 1.3×10^7 m^{-1}.

The difference between the rotating and non-rotating attractive BEC systems is the swallowtail structure's dependence on the band index. In a rotating attractive BEC with the repulsive DDI, the swallowtail lengthens with increasing band index, and in a non-rotating attractive BEC system, the swallowtail shrinks with increasing band index. For the rotating system, a longer swallowtail appears around the boundary at the second excited band than around that at the first. Around the center of the third excited band, a solution with a lobed shape instead of a swallowtail structure appears. For the non-rotating system, the swallowtail around the center at the third excited band is shorter than that at the first. Because of merging with the other solution, the swallowtail around the boundary at the second excited band seems slightly longer than that at the first. The insets also show some interesting Bloch functions for an attractive BEC. The Bloch functions at points A and B of the rotating system are similar to that of the non-rotating dipolar BEC system and are not shown in the inset of Figure 7a.

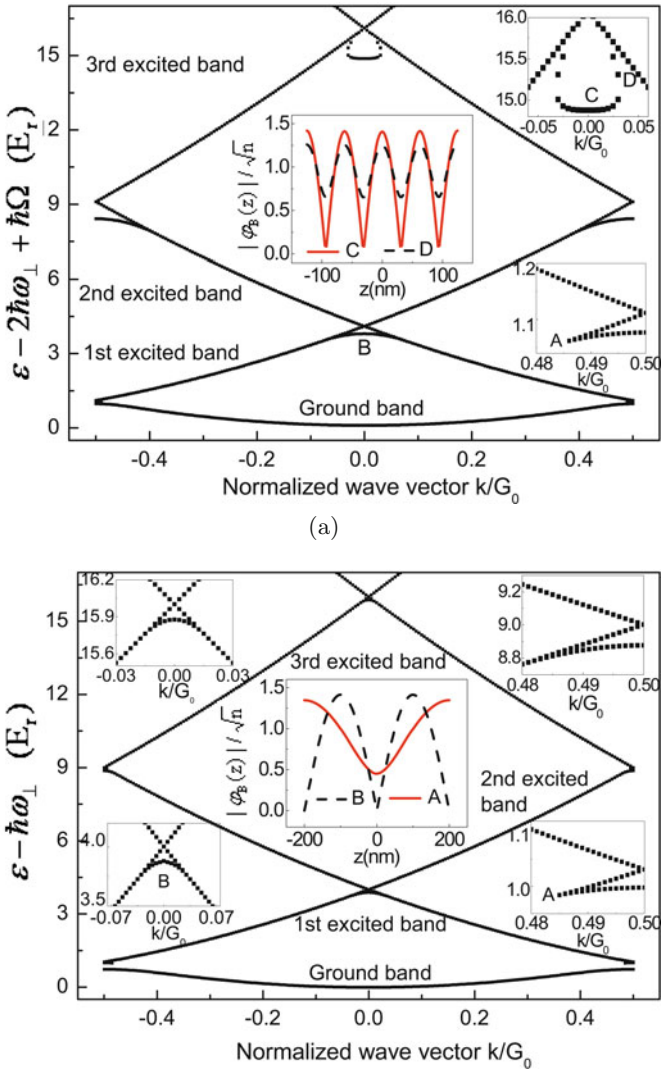

Fig. 7. (Color online) (a) The 5-mode band structure for the rotating dipolar BEC. The BEC is attractive, the DDI is repulsive at $\gamma = 90°$, $a_s = 15a_B$, $a_\perp = 0.523$ μm, $d = 250$ nm, $V_0 = 0.2E_r$, $n = 3n_{c,r}$, and $n_{c,r} = 4.3 \times 10^7$ m^{-1}. (b) The 5-mode band structure for the non-rotating dipolar BEC. The BEC is attractive, the DDI is repulsive at $\gamma = 90°$, $a_s = -1575a_B$, $a_\perp = 0.523$ μm, $d = 400$ nm, $V_0 = 0.5E_r$, $n = 2n_{c,nr}$ and $n_{c,nr} = 1.3 \times 10^7$ m^{-1}. Inset plots show the absolute value of interesting Bloch functions, and enlarged band structures around the zone boundary and zone center.

For a rotating system, if the repulsive DDI is replaced with an attractive DDI in an attractive BEC, the swallowtail structure becomes a shrinking dependence on the band index, which is similar to the repulsive BEC with an attractive DDI replaced by a repulsive DDI; this is demonstrated in Figure 6a and thus not shown again.

So far, we can see that rotation has a significant effect on a dipolar BEC in an optical lattice. First, due to the dipolar rotating term derived from the DDI potential, the definition regarding the type of BEC changes. The type of

Table 1. Swallowtail dependence on the band index for slowly rotating dipolar BEC with a quantized vortex along a 1D optical lattice. The energy of effective contact term overall the space is abbreviated as "effective contact energy", while the energy of dipolar rotating term overall the space is abbreviated as "dipolar rotating energy". "Effective contact energy + dipolar rotating energy" is the sum over the two terms.

DDI type \ BEC type	Repulsive BEC (effective contact energy + dipolar rotating energy) > 0	Attractive BEC (effective contact energy + dipolar rotating energy) < 0
Attractive DDI (dipolar rotating energy) > 0	Elongating swallowtail dependence	Shrinking swallowtail dependence
Repulsive DDI (dipolar rotating energy) < 0	Shrinking swallowtail dependence	Elongating swallowtail dependence

BEC can no longer be determined simply by the s-wave scattering length or the coupling constant of the effective contact interaction, but depends on the dipolar rotating term. The new definition is that if the energy summed over the effective contact term and the dipolar rotating term over all space is positive, the BEC is repulsive; otherwise, the BEC is attractive. One good example appears in Figure 7a. In that case, although the s-wave scattering length is positive, and the DDI is also repulsive, the BEC is still attractive because the negative dipolar rotating term is much stronger than the positive effective contact term. Second, due to the dipolar rotating term, the swallowtail structure no longer always shrinks as the band index increases. The swallowtail can lengthen with increasing band index when the BEC is repulsive and has an attractive DDI, or the BEC is attractive and has a repulsive DDI. Otherwise, for a repulsive (attractive) BEC with a repulsive (attractive) DDI, the swallowtail shrinks as the band index increases. For clarity, the swallowtail dependence on the band index for various types of BEC and DDI is summarized in Table 1.

Before discussing the applications of this flexible swallowtail dependence, we examine the vortex line stability of a dipolar BEC in our calculations by the criterion in reference [44] first. The Wannier function is given by

$$w(\mathbf{r}-\mathbf{R}) = \frac{1}{\sqrt{N_{\text{site}}}} \sum_{\mathbf{k}} e^{-i\mathbf{k}\cdot\mathbf{R}} \Psi_{\mathbf{k}}(\mathbf{r}), \tag{28a}$$

$$\int_{\text{all site}} d\mathbf{r} w^*(\mathbf{r}-\mathbf{R}) w(\mathbf{r}-\mathbf{R}') = \frac{N_{\text{atom}}}{N_{\text{site}}} \sum_{\mathbf{k}} e^{i\mathbf{k}\cdot(\mathbf{R}-\mathbf{R}')} = N_{\text{atom}} \delta_{\mathbf{R},\mathbf{R}'}, \tag{28b}$$

where $\mathbf{R}$ denotes the lattice point. In our case, $\mathbf{R}$ is $\nu d\hat{z}$, where ν is an integer.

The wave function can also be presented by using the Wannier function:

$$\Psi_{\mathbf{k}}(\mathbf{r}) = \frac{1}{\sqrt{N_{\text{site}}}} \sum_{\mathbf{R}} e^{i\mathbf{k}\cdot\mathbf{R}} w(\mathbf{r}-\mathbf{R}), \tag{29a}$$

$$\int_{\text{all site}} d\mathbf{r}\, \Psi^*_{\mathbf{k}}(\mathbf{r})\, \Psi_{\mathbf{k}'}(\mathbf{r}) = \frac{N_{\text{atom}}}{N_{\text{site}}} \sum_{\mathbf{R}} e^{i(\mathbf{k}-\mathbf{k}')\cdot\mathbf{R}} = N_{\text{atom}} \delta_{\mathbf{k},\mathbf{k}'}. \tag{29b}$$

Using the Wannier function associated with the lowest band [44], one can calculate

$$\tilde{g} = g_s d \int_{-d/2}^{d/2} w^4(z) dz + g_d d^{-1} \sum_{\nu\neq 0} |W(\nu G_0)|^2 \equiv \tilde{g}_s + \tilde{g}_d, \tag{30a}$$

$$J = \frac{1}{nd} \int_{-d/2}^{d/2} w(z) \left[-\frac{\hbar^2}{2m} \frac{d^2}{dz^2} + V_0 \sin^2\left(\frac{\pi z}{d}\right) \right] w(z+d) dz, \tag{30b}$$

where $W(\nu G_0)$ is the Fourier transform of $w(z)$. With $\tilde{g}$ and J, the ratio $\beta = g_d/\tilde{g}$ and the effective mass $m^* = \hbar^2/(2d^2 J)$ can be calculated to examine the vortex stability [44]. When both $-1 < \beta < 0$ and $m^* > m$ hold, the vortex could be unstable. Since the scattering lengths a_s for a rotating dipolar BEC in our calculations are all positive, the ratio β is positive, and the vortex does not enter the unstable region. When the Wannier function is assumed [45] as $\varphi_{B,k=0}(z) \sin c(z+\nu d)$, the calculated effective mass m^* in our results is hundred times lower than ^{52}Cr mass m. Hence, even if the scattering length a_s is negative, the vortex in our case is also stable.

Reference [44] also gives a criterion for the phonon's instability ($\beta < -1$ or $\beta > 2$) when the optical lattice is strong. However, due to the swallowtail criterion $n > \frac{V_0}{|2(g_{eff} - g_{rot} G_0^2)|}$, the optical lattice in our calculation was kept weak; otherwise, the atom density becomes too high. Thus, the criterion in reference [44] was not valid for our results, and the phonon's stability should be examining by using the Bogoliubov de Gennes (BdG) equation, which is derived in Appendix B and can be expressed as

see equations (31a) and (31b) in next page

where $\varphi_k = \varphi_{B,k}(z)$ is the condensate's Bloch function at the wave vector k. ω_{kq} denotes the phonon's energy, where q is the phonon's wave vector, while $u_{kq}(z)$ and $v_{kq}(z)$ are the phonon's Bloch functions. Note that terms with g_{rot} result from the dipolar rotating term in equation (21). As $u_{kq}(z)$ and $v_{kq}(z)$ are expanded as a 3-mode Fourier series, equations (31a) and (31b) becomes a 6×6 matrix equation (shown in Appendix B), where we can see that the matrix is much more complex than that of a non-rotating dipolar system due to the dipolar rotating term. At present, while the Landau damping and dynamical instability around the Brillouin zone boundary for a non-rotating non-dipolar system was indicated [28,29], the effect of DDI on the phonon's stability at swallowtails even

$$\left\{\frac{\hbar^2}{2m}\left(-i\frac{d}{dz}+k+q\right)^2+V_0\sin^2\left(\frac{\pi z}{d}\right)+2g_{eff}|\varphi_k|^2-\mu+2\hbar\omega_\perp-\hbar\Omega\right.$$
$$\left.+g_{rot}\left[\frac{d^2}{dz^2}|\varphi_k|^2+\varphi_k\left(\frac{d}{dz}+iq\right)^2\varphi_k^*+2\varphi_k\left(\frac{d}{dz}+iq\right)\varphi_k^*\frac{d}{dz}+|\varphi_k|^2\frac{d^2}{dz^2}\right]\right\}u_{kq}(z)$$
$$+\left\{g_{eff}\varphi_k^2+g_{rot}\left[\varphi_k\left(\frac{d}{dz}+iq\right)^2\varphi_k+2\varphi_k\left(\frac{d}{dz}+iq\right)\varphi_k\frac{d}{dz}+\varphi_k^2\frac{d^2}{dz^2}\right]\right\}v_{kq}(z)=\hbar\omega_{kq}u_{kq}(z) \quad (31a)$$

$$\left\{\frac{\hbar^2}{2m}\left(-i\frac{d}{dz}-k+q\right)^2+V_0\sin^2\left(\frac{\pi z}{d}\right)+2g_{eff}|\varphi_k|^2-\mu+2\hbar\omega_\perp-\hbar\Omega\right.$$
$$\left.+g_{rot}\left[\frac{d^2}{dz^2}|\varphi_k|^2+\varphi_k^*\left(\frac{d}{dz}+iq\right)^2\varphi_k+2\varphi_k^*\left(\frac{d}{dz}+iq\right)\varphi_k\frac{d}{dz}+|\varphi_k|^2\frac{d^2}{dz^2}\right]\right\}v_{kq}(z)$$
$$+\left\{g_{eff}\varphi_k^{*2}+g_{rot}\left[\varphi_k^*\left(\frac{d}{dz}+iq\right)^2\varphi_k^*+2\varphi_k^*\left(\frac{d}{dz}+iq\right)\varphi_k^*\frac{d}{dz}+\varphi_k^{*2}\frac{d^2}{dz^2}\right]\right\}u_{kq}(z)=-\hbar\omega_{kq}v_{kq}(z) \quad (31b)$$

in the non-rotating system has not been understood [46]. Therefore, a numerical calculation of the phonon's issue in both the non-rotating and rotating dipolar systems is needed, and the systematical study is left in another work.

The flexible swallowtail dependence is helpful for studying the dynamics of a BEC in its band structures. Unlike an electron in crystal, which can be subject to an electric field, the driving force of atoms can be implemented using an accelerating optical lattice. After the driving force is applied to the atom, the atom accelerates, and thus the wave vector k increases. When the atom passes the zone boundary designated as point x in the inset of Figure 2, the atom does not go to point y' but moves up to point y; thus, Bloch oscillation fails. If the external force is strong enough, the atom will jump to point z at a higher band, which is the so-called Landau-Zener tunneling [18,19]. The Landau-Zener tunneling rate depends on the gap between the tip of the swallowtail (point y) and the higher band (point z). Due to the flexible swallowtail structure, the gap size in a rotating system can be more easily adjusted than that in a non-rotating system, which thus offers advantages for the experimental demonstration of Landau-Zener tunneling.

Landau-Zener tunneling behavior in the weak and strong nonlinear regimes is very different [18,19]. In the weak regime (i.e., no swallowtail appears), the Landau-Zener tunneling rate depends on $\exp[-\pi q_f E_g^2/2\alpha_s]$, where E_g is the energy gap between the two bands, α_s is the sweeping rate of the accelerating field, and q_f is a factor [18,19]. Hence, in the adiabatic limit ($\alpha_s = 0$), the tunneling rate becomes zero. However, when the nonlinearity is strong enough (i.e., swallowtail appears), the tunneling rate in the adiabatic limit still has a finite value. Because the contact interaction of a rotating BEC is half that of a non-rotating BEC, rotation provides an opportunity to examine the tunneling difference between the two regimes even in the absence of DDI. We can design a system in which rotating and non-rotating BECs are in the weak and strong regimes, respectively, and then measure such a tunneling difference using only rotation, without changing the scattering length a_s or the lattice amplitude V_0. If the DDI is further considered, the dipolar rotating term is involved apart from the dipolar contact term, which thus offers a greater degree of freedom to tune the tunneling regimes.

These various swallowtail structures can also be applied to study intra (inter) subband dynamics in a BEC. In semiconductors, an electron confined in a quantum well can have a series of subbands, where intra (inter) subband dynamics has been extensively studied and applied to optoelectronics such as infrared photodetectors. Although a BEC cannot have such a series of subbands due to quantum confinement, the swallowtail energy structure is very similar to the subbands of an electron in a quantum well. While the state of the swallowtail structure may show Landau damping or dynamical instability [47,48], the corresponding damping time [49] is much longer than an intra (inter) subband transition time [50,51], which thus can be resolved. By pumping an atom to the upper swallowtail subband, scatterings in the same subband (intrasubband) and the transition from the upper to lower swallowtail subbands (intersubband) can be studied. Since rotation can produce various swallowtail structures, it is helpful to design band structures to explore such subband dynamics within current technologies.

Swallowtail structures are also related to solitons due to the nonlinear interaction, which compensates for dispersion; thus, a wave can propagate without spreading. A nonlinear Kerr medium offers a nice analog to a BEC if a Kerr coefficient n_2 (i.e., intensity-dependent index) [52] is drawn parallel to an s-wave scattering length. A positive (negative) Kerr coefficient corresponds to a negative

(positive) s-wave scattering length. Accordingly, atomic bright (dark) solitons occur in attractive (repulsive) BECs without an optical lattice, where a dark soliton propagates with a density dip. If a BEC is subjected to optical lattices, gap solitons may occur around the bandgap where the band curvature (effective mass) is negative [31,32]. Since the band curvature around swallowtails is positive, gap solitons cannot be generated there. However, under rotation, an interesting experiment can be designed. By using the flexible swallowtail dependence on the band index, one can design a band structure in which the effective mass is negative around the bandgap at the lowest band while swallowtails exist at higher bands. Thus, the gap soliton survives at the lowest band, and the effect of swallowtails at the higher band on the gap soliton can be studied. The role of the dipolar rotating term in dispersion compensation can also be understood.

5 Conclusions

Rotation in the presence of quantized vortices is a unique feature of superfluids. Due to the technology of optical lattices, a BEC can exhibit a seemingly contradictory phenomenon that never occurs in helium superfluid; i.e., the BEC density subject to the optical lattice is modulated periodically, but the BEC can rotate around the optical lattice at the same time. For a slowly rotating system, the band structure of a BEC with a quantized vortex along a 1D lattice becomes interesting when DDI is involved or the effective GPEs of the rotating and non-rotating systems do not differ much. Under rotation, a dipolar rotating term can be derived from the DDI potential in the effective GPE and shows an intriguing property. The dipolar rotating term makes a BEC with an attractive DDI more stable than that with a repulsive DDI, which is counterintuitive and also contrary to the conventional effective contact term. The dipolar rotating term changes and generalizes the definition for the type of BEC; the band structure becomes more tunable than that of a non-rotating dipolar BEC system. By adjusting the relationship between the dipolar rotating term and the effective contact term, various swallowtail structures can be achieved, and an attractive BEC without collapse can be easily obtained, facilitating the exploration of atom dynamics in band structures, gap solitons, and strongly correlated (super) TG gas. Furthermore, in the same configuration of the optical lattice, when the rotation accelerates so that a single quantized vortex becomes a vortex lattice, more interesting physics can be expected. The corresponding band structures can be extensively applied to the integer or fractional (strongly correlated) quantum Hall fluids and the debate regarding the validity of the Kolmogorov law for quantum turbulence.

The work is financially supported by a project of the National Science Council, Taiwan under numbers NSC 97-2811-M-009-055 and NSC 97-2112-M-009-002-MY3.

Appendix A: Translation symmetry in a band structure

Consider a Hamiltonian $H = -\frac{\hbar^2}{2m}\frac{d^2}{dz^2} + U(z)$, where $U(z)$ is periodic and can be expressed as $U(z) = \sum_G U_G e^{iGz}$, where $G = \nu G_0$ and ν is an integer. The wave function $\varphi(z)$ can be expressed as a Fourier series summed over all wave vectors permitted by the boundary conditions

$$\varphi(z) = \sum_k c(k) e^{ikz}. \tag{A.1}$$

Substituting $\varphi(z)$ as shown in (A.1) into the Hamiltonian given above yields

$$\sum_k \frac{\hbar^2}{2m} k^2 c(k) e^{ikz} + \sum_G \sum_k U_G c(k-G) e^{i(k+G)z} = \varepsilon \sum_k c(k) e^{ikz}. \tag{A.2}$$

Comparing the coefficients on either side of (A.2) for each Fourier component yields a corresponding central equation:

$$\left(\frac{\hbar^2 k^2}{2m} - \varepsilon\right) c(k) + \sum_G U_G c(k-G) = 0. \tag{A.3}$$

Due to the periodicity in (A.3), the $\varphi(z)$ shown in (A.1) can then be expressed as

$$\varphi_k(z) = \sum_G c(k-G) e^{i(k-G)z} = e^{ikz} \left(\sum_G c(k-G) e^{-iGz}\right) = e^{ikz} \varphi_B(z), \tag{A.4}$$

where $\varphi_B(z) \equiv \sum_G c(k-G) e^{-iGz}$ is the Bloch function.

Therefore, with a G_0 translation, the wave function can be expressed as

$$\varphi_{k+G_0}(z) = e^{i(k+G_0)z} \sum_G c(k+G_0-G) e^{-iGz} = e^{ikz} \sum_{G'} c(k-G') e^{-iG'z} = e^{ikz} \varphi_B(z) = \varphi_k(z), \tag{A.5}$$

where $G' = G - G_0$. The G_0 translation symmetry of the wave function is proven.

$$\begin{pmatrix} H_{11}^{nr}+H_{11}^{r}-\mu+2\hbar\omega_\perp-\hbar\Omega & g_{eff}\varphi_k^2+H_{12}^{r} \\ -g_{eff}\varphi_k^{*2}-H_{21}^{r} & -H_{22}^{nr}-H_{22}^{r}+\mu-2\hbar\omega_\perp+\hbar\Omega \end{pmatrix} \begin{pmatrix} u_{kq}(z) \\ v_{kq}(z) \end{pmatrix} = \hbar\omega_{kq} \begin{pmatrix} u_{kq}(z) \\ v_{kq}(z) \end{pmatrix} \tag{B.4}$$

Appendix B: BdG equation for a slowly rotating dipolar BEC with a vortex along a 1D optical lattice

We start from the time-dependent GPE,

$$i\hbar\partial_t\Psi(\mathbf{r},t) = \left[\frac{-\hbar^2}{2m}\nabla^2+\frac{1}{2}m\omega_\perp^2\rho^2+V_0\sin^2\left(\frac{\pi z}{d}\right)-\Omega L_z +g_s|\Psi(\mathbf{r},t)|^2+g_d\int d^3\mathbf{r}'V_d(\mathbf{r},\mathbf{r}')|\Psi(\mathbf{r}',t)|^2\right]\Psi(\mathbf{r},t), \tag{B.1}$$

where $\Psi(\mathbf{r},t)$ can be written as $\psi_\perp(\rho,\phi)\varphi(z,t)$. Multiplying (B.1) by $\psi_\perp(\rho,\phi)$ and then integrating it over the transverse cross section spanned by $\rho\,d\rho\,d\phi$ yields

$$i\hbar\partial_t\varphi(z,t)+(\hbar\Omega-2\hbar\omega_\perp)\varphi(z,t) = \left[\frac{-\hbar^2}{2m}\partial_z^2+V_0\sin^2\left(\frac{\pi z}{d}\right)+g_{eff}|\varphi(z,t)|^2 + g_{rot}\partial_z^2|\varphi(z,t)|^2\right]\varphi(z,t). \tag{B.2}$$

The time-dependent axial wave function can be written as

$$\varphi(z,t) = e^{-i\frac{\mu}{\hbar}t}e^{ikz}\left[\varphi_k(z)+\sum_q u_{kq}(z)e^{iqz}e^{-i\omega_{kq}t} + v_{kq}^*(z)e^{-iqz}e^{i\omega_{kq}^*t}\right], \tag{B.3}$$

where the condensate's Bloch function $\varphi_k(z)$ was solved in Section 3. The phonon's energy ω_{kq} and its Bloch functions, $u_{kq}(z)$ and $v_{kq}(z)$, are to be solved. If ω_{kq} is real and negative, the condensate may show Landau damping or Beliaev damping, depending on the condensate's temperature [46]. If ω_{kq} is complex and the imaginary part is positive, the condensate will be dynamically unstable due to an exponential growth, which the instability can occur even at the zero temperature.

Substituting (B.3) into (B.2) yields the BdG equation in matrix form,

see equation (B.4) above

which is equivalent to equations (31a) and (31b), where the non-rotating Hamiltonian

$$H_{11,22}^{nr} = \frac{\hbar^2}{2m}\left(-i\frac{d}{dz}\pm k+q\right)^2+V_0\sin^2\left(\frac{\pi z}{d}\right)+2g_{eff}|\varphi_k|^2,$$

the rotating Hamiltonian

$$H_{11,22}^{r} = g_{rot}\left[\frac{d^2}{dz^2}|\varphi_k|^2+\varphi_k^{'*}\left(\frac{d}{dz}+iq\right)^2\varphi_k^{*,} + 2\varphi_k^{'*}\left(\frac{d}{dz}+iq\right)\varphi_k^{*,}\frac{d}{dz}+|\varphi_k|^2\frac{d^2}{dz^2}\right]$$

and

$$H_{12,21}^{r} = g_{rot}\left[\varphi_k^{'*}\left(\frac{d}{dz}+iq\right)^2\varphi_k^{'*} + 2\varphi_k^{'*}\left(\frac{d}{dz}+iq\right)\varphi_k^{'*}\frac{d}{dz}+\left(\varphi_k^{'*}\right)^2\frac{d^2}{dz^2}\right],$$

where the compact form $\varphi_k^{'*}$ denotes φ_k and φ_k^*, respectively, and so is $\varphi_k^{*,}$ for φ_k^* and φ_k. The BdG equation for the non-rotating dipolar system can be also presented as (B.4) where $g_{rot}=0$, $\Omega=0$, $2\hbar\omega_\perp$ is replaced with $\hbar\omega_\perp$, and g_{eff} is replaced with $g_{eff}^{(nr)}$.

The Bloch function $u_{kq}(z)$ and $v_{kq}(z)$ can be expanded in a Fourier's series,

$$u_{kq}(z) = \sqrt{n}\sum_{\nu=-M'}^{M'}\tilde{u}_\nu\exp(i\nu G_0 z),$$

$$v_{kq}(z) = \sqrt{n}\sum_{\nu=-M'}^{M'}\tilde{v}_\nu\exp(i\nu G_0 z), \tag{B.5}$$

where M' must be less than M (the number for a condensate's Bloch function) [28,29]. With a 3-mode expansion ($M'=1$), the BdG equation in (B.4) can be rewritten as

$$\mathbf{M}_{\mathrm{BdG}}(\tilde{u}_{-1},\tilde{u}_0,\tilde{u}_1,\tilde{v}_{-1},\tilde{v}_0,\tilde{v}_1)^T = \hbar\omega_{kq}(\tilde{u}_{-1},\tilde{u}_0,\tilde{u}_1,\tilde{v}_{-1},\tilde{v}_0,\tilde{v}_1)^T, \tag{B.6}$$

where $\mathbf{M}_{\mathrm{BdG}}$ is given by

see equation in next page →

$$
\begin{pmatrix}
\frac{\hbar^2}{2m}(G_0-k-q)^2+\frac{V_0}{2} & -\frac{V_0}{4}+n[2Ag_{eff} & n[2Bg_{eff}+g_{rot}(R^{11}_{-11} & n[C(g_{eff}-g_{rot}G_0^2) & n(2D_1g_{eff}+g_{rot}R^{21}_{-10}) & n[E_1(g_{eff}-g_{rot}G_0^2) \\
+n[2g_{eff}+g_{rot}(R^{11}_{-1-1}+R^{12}_{-1-1} & +g_{rot}(R^{11}_{-10}-AG_0^2)] & +R^{12}_{-11}-5BG_0^2)] & +g_{rot}(R^{21}_{-1-1}+R^{22}_{-1-1})] & & +g_{rot}(R^{21}_{-11}+R^{22}_{-11})] \\
-G_0^2)]-\mu+2\hbar\omega_\perp-\hbar\Omega & & & & & \\
-\frac{V_0}{4}+n[2Ag_{eff}+g_{rot}\cdot & \frac{\hbar^2}{2m}(k+q)^2+\frac{V_0}{2}+n(2g_{eff} & -\frac{V_0}{4}+n[2Ag_{eff}+g_{rot}\cdot & n[2D_2(g_{eff}-g_{rot}G_0^2) & n(Cg_{eff}+g_{rot}R^{22}_{00}) & n[2D_1(g_{eff}-g_{rot}G_0^2) \\
(R^{11}_{0-1}+R^{12}_{0-1}-2AG_0^2)] & +g_{rot}R^{11}_{00})-\mu+2\hbar\omega_\perp-\hbar\Omega & (R^{11}_{01}+R^{12}_{01}-2AG_0^2)] & +g_{rot}(R^{21}_{0-1}+R^{22}_{0-1})] & & +g_{rot}(R^{21}_{01}+R^{22}_{01})] \\
n[2Bg_{eff}+g_{rot}(R^{11}_{1-1} & -\frac{V_0}{4}+n[2Ag_{eff} & \frac{\hbar^2}{2m}(G_0+k+q)^2+\frac{V_0}{2} & n[E_2(g_{eff}-g_{rot}G_0^2) & n(2D_2g_{eff}+g_{rot}R^{21}_{10}) & n[C(g_{eff}-g_{rot}G_0^2) \\
+R^{12}_{1-1}-5BG_0^2)] & +g_{rot}(R^{11}_{10}-AG_0^2)] & +n[2g_{eff}+g_{rot}(R^{11}_{11}+R^{12}_{11} & +g_{rot}(R^{21}_{1-1}+R^{22}_{1-1})] & & +g_{rot}(R^{21}_{11}+R^{22}_{11})] \\
 & & -G_0^2)]-\mu+2\hbar\omega_\perp-\hbar\Omega & & & \\
-n[C(g_{eff}-g_{rot}G_0^2) & -n(2D_2g_{eff}+g_{rot}S^{21}_{-10}) & -n[E_2(g_{eff}-g_{rot}G_0^2) & -\frac{\hbar^2}{2m}(G_0+k-q)^2-\frac{V_0}{2} & \frac{V_0}{4}-n[2Ag_{eff} & -n[2Bg_{eff}+g_{rot}\cdot \\
+g_{rot}(S^{21}_{-1-1}+S^{22}_{-1-1})] & & +g_{rot}(S^{21}_{-11}+S^{22}_{-11})] & -n[2g_{eff}+ng_{rot}(S^{11}_{-1-1}+S^{12}_{-1-1} & +g_{rot}(S^{11}_{-10}-AG_0^2)] & (S^{11}_{-11}+S^{12}_{-11}-5BG_0^2)] \\
 & & & -G_0^2)]+\mu-2\hbar\omega_\perp+\hbar\Omega & & \\
-n[2D_1(g_{eff}-g_{rot}G_0^2) & -n(Cg_{eff}+g_{rot}S^{21}_{00}) & -n[2D_2(g_{eff}-g_{rot}G_0^2) & \frac{V_0}{4}-n[2Ag_{eff}+g_{rot}\cdot & -\frac{\hbar^2}{2m}(k-q)^2-\frac{V_0}{2}-n(2g_{eff} & \frac{V_0}{4}-n[2Ag_{eff}+g_{rot}\cdot \\
+g_{rot}(S^{21}_{0-1}+S^{22}_{0-1})] & & +g_{rot}(S^{21}_{01}+S^{22}_{01})] & (S^{11}_{0-1}+S^{12}_{0-1}-2AG_0^2)] & +g_{rot}S^{11}_{00})+\mu-2\hbar\omega_\perp+\hbar\Omega & (S^{11}_{01}+S^{12}_{01}-2AG_0^2)] \\
-n[E_1(g_{eff}-g_{rot}G_0^2) & -n(2D_1g_{eff}+g_{rot}S^{21}_{10}) & -n[C(g_{eff}-g_{rot}G_0^2) & -n[2Bg_{eff}+g_{rot}\cdot & \frac{V_0}{4}-n[2Ag_{eff} & -\frac{\hbar^2}{2m}(G_0-k+q)^2-\frac{V_0}{2} \\
+g_{rot}(S^{21}_{1-1}+S^{22}_{1-1})] & & +g_{rot}(S^{21}_{11}+S^{22}_{11})] & (S^{11}_{1-1}+S^{12}_{1-1}-5BG_0^2)] & +g_{rot}(S^{11}_{10}-AG_0^2)] & -n[2g_{eff}+g_{rot}(S^{11}_{11}+S^{12}_{11}-G_0^2)] \\
 & & & & & +\mu-2\hbar\omega_\perp+\hbar\Omega
\end{pmatrix}
$$

$$\begin{pmatrix} R^{11}_{-1-1} = -G_0[4c^2_{-2}(G_0+q) + c^2_{-1}(G_0+2q) & R^{11}_{-10} = -c_{-2}c_{-1}(G_0+q)^2 - c_{-1}c_0q^2 & R^{11}_{-11} = -c_{-2}c_0q^2 - c_{-1}c_1(G_0-q)^2 \\ +c^2_1(G_0-2q) + 4c^2_2(G_0-q)] - q^2 & -c_0c_1(G_0-q)^2 - c_1c_2(2G_0-q)^2 & -c_0c_2(2G_0-q)^2 \\ R^{11}_{0-1} = -c_{-2}c_{-1}(2G_0+q)^2 - c_{-1}c_0(G_0+q)^2 & R^{11}_{00} = R^{11}_{-1-1} & R^{11}_{01} = R^{11}_{-10} \\ -c_0c_1q^2 - c_1c_2(G_0-q)^2 & & \\ R^{11}_{1-1} = -c_{-2}c_0(2G_0+q)^2 & R^{11}_{10} = R^{11}_{0-1} & R^{11}_{11} = R^{11}_{-1-1} \\ -c_{-1}c_1(G_0+q)^2 - c_0c_2q^2 & & \end{pmatrix}$$

$$\begin{pmatrix} R^{12}_{-1-1} = 2G_0[G_0(2c^2_{-2} + c^2_{-1} - c^2_1 - 2c^2_2) + q] & R^{12}_{-10} = 0 & R^{12}_{-11} = -2G_0[c_{-2}c_0q - c_{-1}c_1(G_0-q) \\ & & -c_0c_2(2G_0-q)] \\ R^{12}_{0-1} = 2G_0[c_{-2}c_{-1}(2G_0+q) + c_{-1}c_0(G_0+q) & R^{12}_{00} = 0 & R^{12}_{01} = -2G_0[c_{-2}c_{-1}(G_0+q) + c_{-1}c_0q \\ +c_0c_1q - c_1c_2(G_0-q)] & & -c_0c_1(G_0-q) - c_1c_2(2G_0-q)] \\ R^{12}_{1-1} = 2G_0[c_{-2}c_0(2G_0+q) & R^{12}_{10} = 0 & R^{12}_{11} = -R^{12}_{-1-1} \\ +c_{-1}c_1(G_0+q) + c_0c_2q] & & \end{pmatrix}$$

$$\begin{pmatrix} R^{21}_{-1-1} = -2c_{-2}c_2(4G_0^2 + q^2) & R^{21}_{-10} = -c_{-2}c_1[G_0(5G_0-2q) + 2q^2] & R^{21}_{-11} = -c^2_{-1}(G_0-q)^2 \\ -2c_{-1}c_1(G_0^2+q^2) - c_0^2q^2 & -c_{-1}c_0[G_0(G_0-2q) + 2q^2] & -2c_{-2}c_0[2G_0(G_0-q) + q^2] \\ R^{21}_{0-1} = -c_{-1}c_2[G_0(5G_0+2q) + 2q^2] & R^{21}_{00} = R^{21}_{-1-1} & R^{21}_{01} = R^{21}_{-10} \\ -c_0c_1[G_0(G_0+2q) + 2q^2)] & & \\ R^{21}_{1-1} = -2c_0c_2[2G_0(G_0+q) + q^2] & R^{21}_{10} = R^{21}_{0-1} & R^{21}_{11} = R^{21}_{-1-1} \\ -c^2_1(G_0+q)^2 & & \end{pmatrix}$$

$$\begin{pmatrix} R^{22}_{-1-1} = 2qCG_0 & R^{22}_{-10} = 0 & R^{22}_{-11} = 2E_1G_0(G_0-q) \\ R^{22}_{0-1} = 2D_2G_0(G_0+2q) & R^{22}_{00} = 0 & R^{22}_{01} = 2D_1G_0(G_0-2q) \\ R^{22}_{1-1} = 2E_2G_0(G_0+q) & R^{22}_{10} = 0 & R^{22}_{11} = -R^{22}_{-1-1} \end{pmatrix}$$

where

$$A = c_{-2}c_{-1} + c_{-1}c_0 + c_0c_1 + c_1c_2,$$

$$B = c_0c_{-2} + c_{-1}c_1 + c_0c_2,$$

$$C = 2c_{-2}c_2 + 2c_{-1}c_1 + c_0^2,$$

$$D_1 = c_{-2}c_1 + c_{-1}c_0,$$

$$D_2 = c_{-1}c_2 + c_0c_1,$$

$$E_1 = 2c_{-2}c_0 + c^2_{-1},$$

$$E_2 = 2c_0c_2 + c^2_1,$$

see above equations

where $S^{mm'}_{nn'} = R^{mm'}_{nn'}(c_\nu \leftrightarrow c_{-\nu})$. For example, $S^{11}_{1-1} = -c_{-2}c_0q^2 - c_{-1}c_1(G_0+q)^2 - c_0c_2(2G_0+q)^2$. Both $R^{mm'}_{nn'}$ and $S^{mm'}_{nn'}$ are generated from the dipolar rotating term. Therefore, the BdG matrix for a rotating dipolar BEC with a quantized vortex along a 1D lattice becomes much more complex than that for a non-rotating dipolar system.

References

1. R.J. Donnelly, *Quantized vortices in helium II* (Cambridge university press, New York, 1991)
2. R. Bhat, M. Krämer, J. Cooper, M.J. Holland, Phys. Rev. A **76**, 043601 (2007)
3. A.G. Morris, D.L. Feder, Phys. Rev. A **74**, 033605 (2006)
4. G. Watanabe, G. Baym, C.J. Pethick, Phys. Rev. Lett. **93**, 190401 (2004)
5. N. Regnault, Th. Jolicoeur, Phys. Rev. Lett. **91**, 030402 (2003)
6. S. Viefers, J. Phys. Cond. Mat. **20**, 123202 (2008)
7. H.L. Stormer, D.C. Tsui, A.C. Gossard, Rev. Mod. Phys. **71**, S298 (1999)

8. W.F. Vinen, J.J. Niemela, J. Low Temp. Phys. **128**, 167 (2002)
9. W.F. Vinen, J. Low Temp. Phys. **145**, 7 (2006)
10. V.S. L'vov, S.V. Nazarenko, O. Rudenko, Phys. Rev. B **76**, 024520 (2007)
11. E. Kozik, B. Svistunov, Phys. Rev. Lett. **94**, 025301 (2005)
12. M. Kobayashi, M. Tsubota, Phys. Rev. A **76**, 045603 (2007)
13. M. Kobayashi, M. Tsubota, Phys. Rev. Lett. **94**, 065302 (2005)
14. T.L. Horng, C.H. Hsueh, S.C. Gou, Phys. Rev. A **77**, 063625 (2008)
15. S. Tsuchiya, S. Kurihara, T. Kimura, Phys. Rev. A **70**, 043628 (2004)
16. Q. Gu, K. Bongs, K. Sengstock, Phys. Rev. A **70**, 063609 (2004)
17. R. Barnett, A. Turner, E. Demler, Phys. Rev. Lett. **97**, 180412 (2006)
18. J. Liu, L. Fu, B.Y. Ou, S.G. Chen, D.I Choi, B. Wu, Q. Niu, Phys. Rev. A **66**, 023404 (2002)
19. B. Wu, Q. Niu, Phys. Rev. A **61**, 023402 (2000)
20. A. Griesmaier, J. Werner, S. Hensler, J. Stuhler, T. Pfau, Phys. Rev. Lett. **94**, 160401 (2005)
21. C. Mora, O. Parcollet, X. Waintal, Phys. Rev. B **76**, 064511 (2007)
22. L. Mathey, I. Danshita, C.W. Clark, Phys. Rev. A **79**, 011602(R) (2009)
23. N.R. Cooper, E.H. Rezayi, S.H. Simon, Phys. Rev. Lett. **95**, 200402 (2005)
24. Y.Y. Lin, R.K. Lee, Y.M. Kao, T.F. Jiang, Phys. Rev. A **78**, 023629 (2008)
25. G.E. Astrakharchik, Y.E. Lozovik, Phys. Rev. A **77**, 013404 (2008)
26. R.M. Wilson, S. Ronen, J.L. Bohn, Phys. Rev. A **79**, 013621 (2009)
27. P. Öhberg, L. Santos, Phys. Rev. Lett. **89**, 240402 (2002)
28. M. Machholm, C.J. Pethick, H. Smith, Phys. Rev. A **67**, 053613 (2003)
29. D. Diakonov, L.M. Jensen, C.J. Pethick, H. Smith, Phys. Rev. A **66**, 013604 (2002)
30. B.T. Seaman, L.D. Carr, M.J. Holland, Phys. Rev. A **71**, 033622 (2005)
31. B. Eiermann, T. Anker, M. Albiez, M. Taglieber, P. Treutlein, K.-P. Marzlin, M.K. Oberthaler, Phys. Rev. Lett. **92**, 230401 (2004)
32. E.A. Ostrovskaya, Y.S. Kivshar, Phys. Rev. Lett. **90**, 160407 (2003)
33. M.A. Baranov, Phys. Rep. **464**, 71 (2008)
34. T.F. Jiang, W.C. Su, Phys. Rev. A **74**, 063602 (2006)
35. A.L. Fetter, A.A. Svidzinsky, J. Phys. Cond. Mat. **13**, R135 (2001)
36. K. Góral, K. Rzażewski, T. Pfau, Phys. Rev. A **61**, 051601 (2000)
37. C. Kittel, *Introduction to solid state physics*, 8th edn. (John Wiley & Son, New York, 2005)
38. Stuhler, A. Griesmaier, T. Koch, M. Fattori, T. Pfau, S. Giovanazzi, P. Pedri, L. Santos, Phys. Rev. Lett. **95**, 150406 (2005)
39. The memory effect mentioned here differs from the non-Markovian process also called the memory effect of quantum kinetics; see H.C. Lee, Phys. Stat. Sol. **245**, 707 (2008) and references [40,41]
40. I. Knezevic, D.K. Ferry, Phys. Rev. E **67**, 066122 (2003)
41. H.C. Lee, C.Y. Mou, Eur. Phys. J. B **73**, 229 (2010)
42. E.J. Mueller, Phys. Rev. A **66**, 063603 (2002)
43. B.G. Streetman, S. Banerjee, *Solid State Electronic Devices*, 6th edn. (Prentice Hall, London, 2006), Chap. 10
44. M. Klawunn, R. Nath, P. Pedri, L. Santos, Phys. Rev. Lett. **100**, 240403 (2008)
45. see p. 267 of reference [37]
46. O. Morsch, M. Oberthaler, Rev. Mod. Phys. **78**, 179 (2006)
47. K. Iigaya, S. Konabe, I. Danshita, T. Nikuni, Phys. Rev. A **74**, 053611 (2006)
48. S. Giorgini, Phys. Rev. A **57**, 2949 (1998)
49. B. Wu, Q. Niu, Phys. Rev. A **64**, 061603 (2001)
50. In GaAs/AlGaAs quantum wells, the intersubband relaxation time is in the picosecond scale quoted from K.W. Sun, C.L. Huang, G.B. Huang, H.C. Lee, Solid State Commun. **126**, 519 (2003) and reference [51]
51. H.C. Lee, K.W. Sun, Microelectr. J. **34**, 671 (2003) 39a
52. Y.S. Kivshar, B.L. Davies, Phys. Rep. **298**, 81 (1998)